Embedded 3D Printing of Strain Sensors within Highly Stretchable Elastomers

Joseph T. Muth, Daniel M. Vogt, Ryan L. Truby, Yiğit Mengüç, David B. Kolesky, Robert J. Wood, and Jennifer A. Lewis**

Since the advent of electronics, advances in fabrication techniques have driven the development of smaller, faster, and more efficient devices. To date, the primary focus has been on rigid electronics. Recent interest in wearable electronics,[1–6] human/machine interfaces,[7,8] and soft robotics,[9–12] among other areas,[13–22] has led to an entirely new class of electronic devices – known as stretchable electronics. These emerging devices require new fabrication schemes that enable integration of heterogeneous soft functional materials.[23,24] One device of particular interest is strain sensors that are enveloped in arbitrarily shaped soft matrices, which are both highly conformal and extensible.[1,4,25–28]

Due to the disparate mechanical properties of soft objects and conventional rigid electronics, integrating electronic devices within highly stretchable matrices has proven difficult. Soft sensors are typically composed of a deformable conducting material patterned onto, attached to, or encapsulated within an inactive stretchable material. To create the desired sensing geometry, a number of processing methods have been employed to date, including lithographic,[5,7,29–32] planar printing,[14,27,33–35] coating,[36–39] and micro-channel molding, filling, and lamination[40–44] techniques. While these methods are effective at creating sensors, problems such as limited extensibility, high cost, poor durability, or lack of manufacturing scalability have prevented their widespread adoption.

Here, we report a new method, known as embedded 3D printing (e-3DP), for fabricating strain sensors within highly conformal and extensible elastomeric matrices (**Figure 1**, Movie S1). This method involves extruding a viscoelastic ink through a deposition nozzle directly into an elastomeric reservoir. The ink forms a resistive sensing element, while the reservoir serves as a matrix material. As the nozzle translates through the reservoir, void space is introduced, which must be filled by a capping (filler fluid) layer.[45] After printing, the reservoir and filler fluid are co-cured to form a monolithic part, while the embedded conductive ink remains fluid. Using e-3DP, soft sensors can be created in a highly programmable and seamless manner. The exquisite print path control, coupled with the supporting reservoir, enable free-form fabrication of nearly arbitrary sensor geometries in planar and 3D motifs. By eliminating interfaces that give rise to delamination between individual layers, their mechanical reliability is significantly improved.

To enable e-3DP, we developed a multicomponent materials system composed of an ink, reservoir, and filler fluid. These constituents are tailored to exhibit the desired rheological properties required to maintain high-fidelity geometries throughout the embedded printing and curing process. In addition, they must be chemically compatible as well as exhibit appropriate mechanical and electrical properties to yield soft devices. We used carbon conductive grease, an off-the-shelf, inexpensive, environmentally benign suspension of carbon black particles in silicone oil as the functional ink for patterning sensing elements within our 3D printed devices. Conductive carbon grease exhibits the requisite rheological characteristics for e-3DP (**Figure 2**). This viscoelastic ink exhibits a strong shear thinning response, in which the apparent viscosity decreases from 10^4 Pa·s to 10 Pa·s as the shear rate increases from 10^{-2} s^{-1} to 10^3 s^{-1}, allowing it to be extruded through fine deposition nozzles. Printing is further facilitated by its yielding behavior. Above the shear yield stress ($\tau_y \sim 10^2$ Pa), its shear elastic modulus (G') drops dramatically with increased shear stress, allowing the ink to be printed at modest pressures. However, below the yield point, the ink possesses a shear elastic modulus of approximately 10^5 Pa, enabling the ink to maintain its filamentary shape after it exits the nozzle.

Several criteria must be fulfilled when designing an appropriate supporting reservoir and filler fluid for e-3DP. First, the reservoir must facilitate patterning the desired ink filaments without breakup. Second, any defects that arise during printing as the nozzle translates within the reservoir must be rapidly healed by incorporation of the filler fluid. Finally, after printing the embedded sensing elements, the infilled reservoir must be transformed by curing into a monolithic, highly extensible, conformal elastomer matrix. To meet these requirements, we modified a commercially available silicone elastomer, Ecoflex 00-30, to create both the reservoir and filler fluid. Specifically, we add thickening and thinning agents to uncured Ecoflex to tailor their respective rheological properties. Upon modification, the reservoir possesses shear thinning behavior (Figure 2a), a τ_y below that of the conductive ink (Figure 2b) to accommodate nozzle translation, a sufficiently high G' value (~10^4 Pa) to support the patterned ink filaments without distorting their geometry, and an ability to be cured after printing is completed. The addition of the thinning agent produces a filler fluid that exhibits nearly Newtonian behavior with a viscosity slightly

J. T. Muth,[+] R. L. Truby, D. B. Kolesky, Prof. J. A. Lewis
Pierce Hall Rm 221, 29 Oxford Street, Cambridge
MA 02138, USA
E-mail: jalewis@seas.harvard.edu
D. M. Vogt,[+] Y. Mengüç, Prof. R. J. Wood
60 Oxford street, Cambridge
MA 02138, USA
E-mail: rjwood@eecs.harvard.edu
[+]The first two authors contributed equally to this work.

DOI: 10.1002/adma.201400334

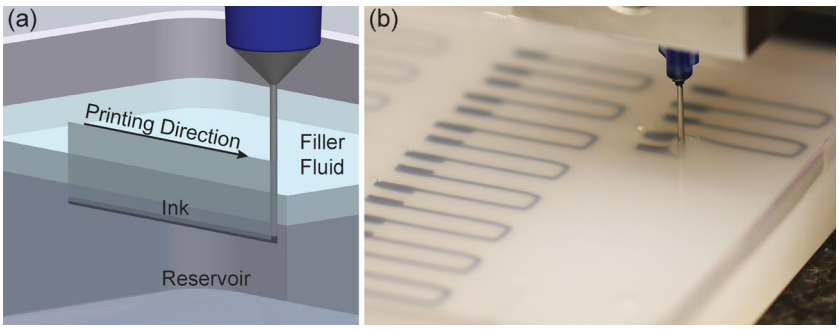

Figure 1. (a) Schematic illustration of the embedded 3D printing (e-3DP) process. A conductive ink is printed into an uncured elastomeric reservoir, which is capped by filler fluid. (b) Photograph of e-3DP for a planar array of soft strain sensors.

above 10 Pa·s over the entire shear rate range tested (Figure 2a) and a corresponding low G' value (<1 Pa) (Figure 2b), which allows the filler fluid to readily flow into and fill the voids that arise as the nozzle is translated through the matrix during the printing process.

Materials compatibility is another important consideration for successful e-3DP of soft sensor devices. The engineered materials set must therefore meet two additional criteria: (1) the conductive ink should minimally dissociate or diffuse within the reservoir both during and after printing to maintain high fidelity features and (2) the reservoir and filler should be identical chemically to eliminate internal interfaces in the elastomeric matrix after curing. Direct observation of the resistive ink within the supporting reservoir indicates that the patterned features do retain their form during the printing and curing processes. Figure S1 confirms the ink remains stable with time after being embedded within the elastomeric matrix. The modifiers added to create the uncured Ecoflex-based reservoir and filler fluid only affect their rheological properties in the pre-cured state. Upon curing, monolithic, highly extensible, conformal sensors are produced. Importantly, the cured elastomeric matrix exhibits large extensibility (up to 900% elongation at break) and softness (Shore Hardness 00–30), making it ideally suited for conformal soft sensing devices.[46]

To demonstrate e-3DP, we fabricated strain sensors of varying geometry embedded within Ecoflex. The sensor design is first rendered in CAD/CAM software that controls the nozzle translation (or tool) path during printing. The cross-sectional dimensions of each printed sensor are controlled by adjusting the nozzle size, applied pressure, and printing speed. As one example, the strain sensors shown in **Figure 3**a are printed using a fixed nozzle diameter (D = 410 μm) and applied pressure (P = 50 psi), and varying print speed from 0.5 mm/s to 4 mm/s. Each strain sensor occupies an area that is 4 mm wide by 20 mm in length. They possess a hairpin (U-shape) configuration composed of cylindrical wire-like features truncated with large contact pads (5 mm in length) at each end, which facilitate electrical connections. The respective cross-sectional areas of the printed U-shaped features decrease from 0.71 ± 0.05 mm^2 to 0.066 ± 0.01 mm^2 as the printing speed increases, which in turn leads to an increase in their electrical resistance from 11 ± 2 kΩ to 60 ± 3 kΩ in their native (unstrained) state. As a benchmark, the carbon-based ink possesses a bulk resistivity (117 Ω•cm),[47] which is comparable to other commercially available carbon greases.[48,49] This ink remains electrically stable over time when encapsulated within the cured elastomer (Figure S1). In addition to smaller filament diameters, higher printing speeds resulted in a more pronounced rounding at the corners of the U-shaped sensors, which could be mitigated by decelerating the nozzle speed in the corner regions, i.e., where there is an abrupt change in the printing direction. By using smaller nozzles coupled with higher printing speeds, it is possible to reduce the overall dimensions of these e-3DP strain sensors by an order of magnitude and the filament cross–section by two orders of magnitude.

To investigate their electrical performance as a function of cyclic straining, the embedded strain sensors described above are extended to 100% strain at a crosshead speed of 2.96 mm/s and relaxed back to a zero strain condition at the same rate. This extend-relax cycle is repeated five times for each soft sensor. Sensors with smaller cross-sectional area provide a larger change in resistance for a given strain compared to those with larger cross-sectional areas (Figure 3b; Figure S2a), indicating that the apparent sensor sensitivity can be tuned simply by adjusting the printing speed. The gauge factor of these soft sensors is determined by normalizing the apparent sensor sensitivity with respect to the native resistance of the unstrained sensors. The gauge factor (measured during the loading portion of the cycle) for all sensors collapsed to a single value, 3.8 ± 0.6, which is akin to that reported for conventional metallic strain gauges.[50] However, significant hysteresis is observed during cycling, which has been reported previously for carbon-based resistive sensing elements.[19,51–54] Hysteresis arises due to disparate time scales associated with breakdown and reformation of contacts between carbon particles within the network as well as the inherent hysteresis associated with elastomeric loading.[19,51,54] Because the carbon particle network governs both ink rheology and electrical resistivity, it is possible to probe sensor performance simply by monitoring its rheological behavior as a function of cycle number (Figure 2c). When strained beyond the elastic limit (~0.1% strain), the carbon black network is disrupted, leading to a decrease in the shear elastic modulus and a concomitant rise in electrical resistance – reflecting fewer interparticle contacts. When subjected to 1% strain for 1000 cycles, the shear elastic modulus, G', decreases by roughly 50%. When subjected to 100% strain for the same number of cycles, G' decreases by over an order of magnitude. We note the cross-sectional geometry of these U-shaped sensors may further influence their hysteresis behavior.[55]

Next, we investigated their response to a step strain input. In this measurement, each U-shaped strain sensor is extended to 100% strain at a crosshead speed of 23 mm/s, held at 100% strain for 20 s, and then relaxed to 0% strain (unstrained) state at the same rate. Again, the soft sensors with smaller cross-sectional area exhibited increased sensitivity compared to those printed with larger cross-sectional area (Figure 3c; Figure S2b).

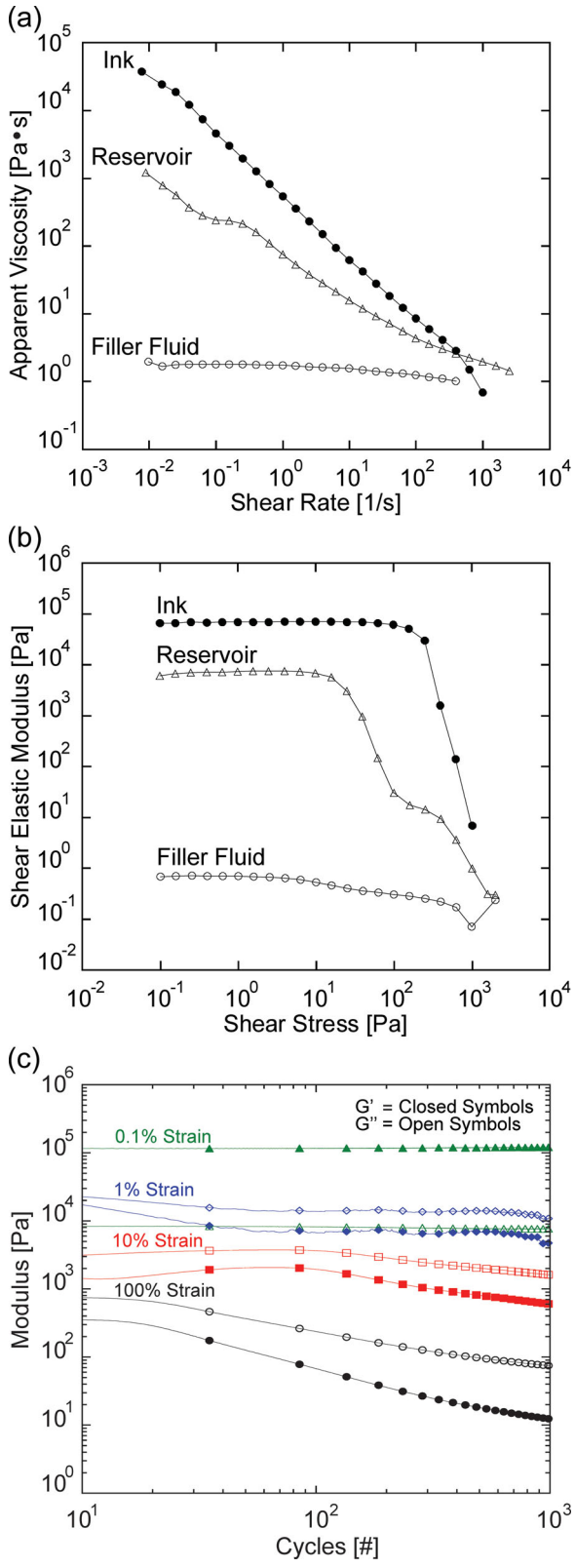

Figure 2. (a) The apparent viscosity as a function of shear rate and (b) the shear elastic modulus as a function of shear stress for the ink, reservoir, and filler fluid. (c) Ink moduli behavior as a function of cycle number for different levels of oscillatory strain.

During step testing, the sensors exhibited overshooting in response to acceleration, followed by relaxation back to a plateau value – a behavior not observed during cyclic testing at lower crosshead speeds. This behavior has also been previously observed.[19] The peaks associated with acceleration are believed to arise from the viscoelastic nature of carbon grease.[53] While the more sensitive sensors appear to suffer from higher acceleration peaks, when peak height is normalized with respect to its plateau level, the relative peak heights between the least and most sensitive sensors, printed at 0.5 mm/s and 4 mm/s, respectively, differ by less than 10%. Similar acceleration effects are observed for step tests to 5% and 50% strain. Only when the ink remains below its yield point is acceleration minimized (Figure S3). Lastly, upon relaxation, the sensors do not recover their initial resistance value. However, for all sensors tested, the final resistance is within 10% of the original value. The difference in the starting and final resistances is attributed to the difference in relaxation time between the cross-linked elastomer (~tens of seconds)[54,56] and the time associated with the re-establishment of filler–filler bonds in the fluid ink (~10's of hours) (Figure S4).

To evaluate their failure strain, we tested five representative strain sensors (printed at 2 mm/s) by extending them at a crosshead speed of 5 mm/s until failure. Each sensor exhibited consistent, predictable electrical response up to ~400% strain (Figure 3d). When extended beyond this value to strains of ~400–700%, their electrical performance is more erratic as a result of percolation network breakdown. Finally, the sensors fail mechanically when extended to strains of ~700–800%. Notably, each sensor fails due to tearing of the interface where the embedded strain sensors are connected to external wires at printed contact pads rather than from defects stemming from the e-3DP process. The above observations reveal that while e-3DP can readily produce highly mechanically robust sensors with tunable properties, further research is needed to further optimize sensor performance and eliminate hysteresis. Alternate inks must be developed that do not rely on conductive particle networks, and printed sensors with ideal cross-sections should be evaluated.[55] Efforts are now underway to explore the use of liquid metals, such as eutectic gallium-indium (e-GaIn), as well as ionic liquids and gels. These materials would allow accurate sensing up to the strain limits set by the encapsulating elastomeric matrix.

To further demonstrate the flexibility of e-3DP, we fabricated large arrays of strain sensors, strain sensors embedded in wearable objects, and multilayer sensing devices. In the first embodiment, we printed a 10×2 array of strain sensors in a 1 mm thick reservoir (Figure S5). These sensors are readily attached to a variety of deformable surfaces including human skin. In another embodiment, we printed strain sensors within a premolded, glove-shaped reservoir (**Figure 4**a), to yield a glove that fits on a user's hand and monitors digit movement. Specifically, we directly printed strain sensors within the glove over the first knuckle regions of each finger. Each sensor is 4 mm wide and 30 mm in length. They are printed using a 410 μm nozzle at 50 psi and a printing speed of 1 mm/s. After curing, the glove is removed from the mold and connected to a data collection system by external wiring. The glove is used to monitor the digit motion of a user in real time (Figure 4b; Movie S2). As a

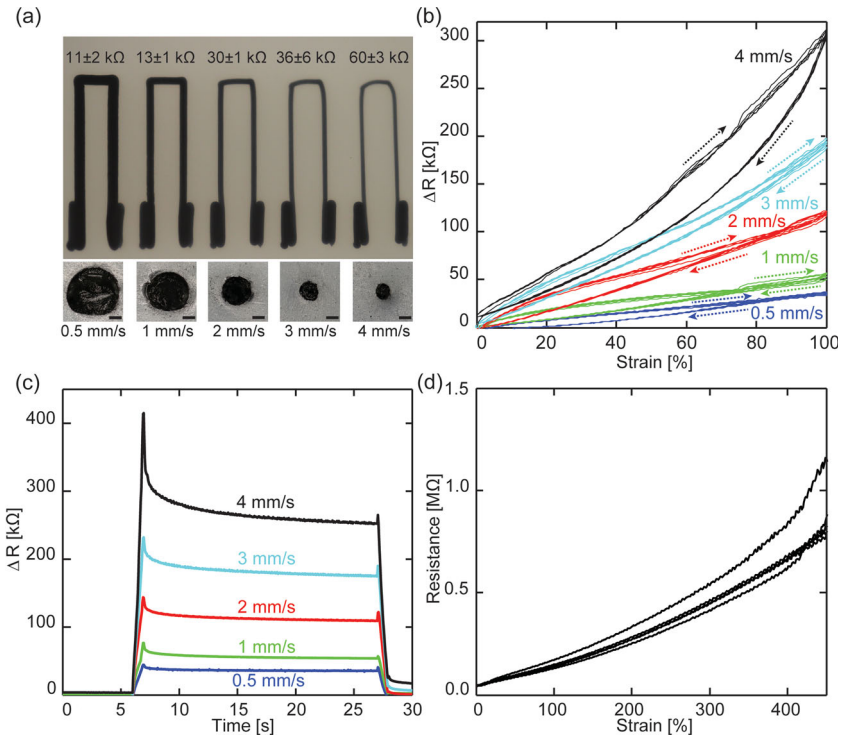

Figure 3. (a) Top and cross-sectional images of soft sensors printed by e-3DP at varying speeds. (b) Electrical resistance change as a function of elongation for sensors subjected to cyclic deformation, in which each sensor is cycled 5 times to 100% strain at a crosshead speed of 2.96 mm/s. (c) Electrical resistance change as a function of time for sensors subjected to step deformation to 100% strain at a crosshead speed of 23 mm/s. (d) Electrical resistance as a function of strain up to 450% strain for sensors strained to mechanical failure at a crosshead speed of 5 mm/s.

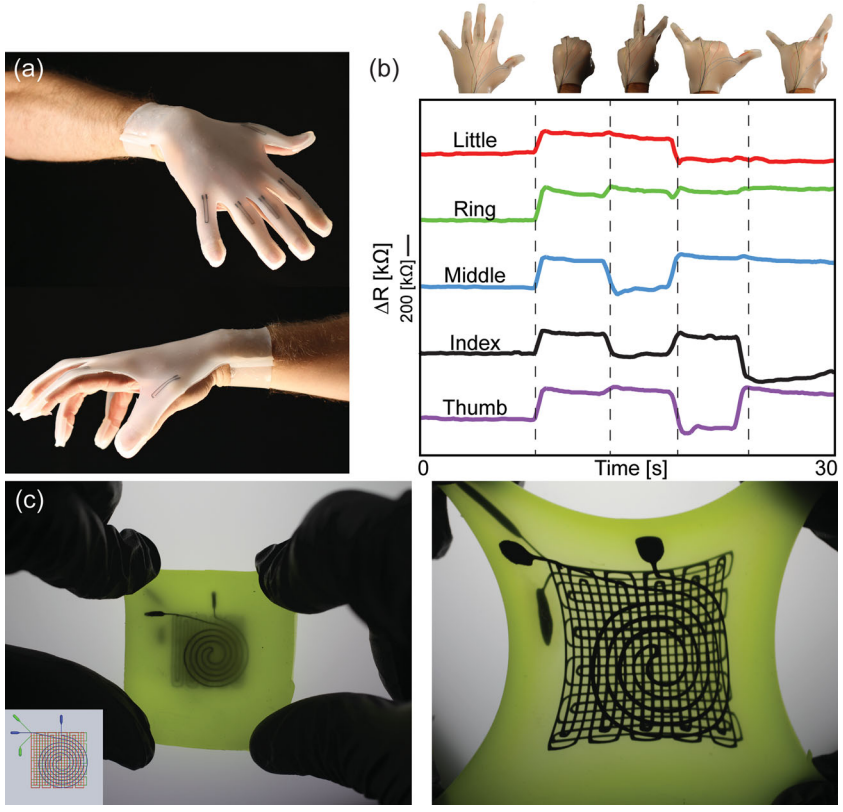

Figure 4. (a) Photograph of a glove with embedded strain sensors produced by e-3DP. (b) Electrical resistance change as a function of time for strain sensors within the glove at five different hand positions. (c) Photograph of a three-layer strain and pressure sensor in the unstrained state (left) and stretched state (right). The top layer consists of a spiral pressure sensor, below which lies a two-layer biaxial strain sensor that consists of two square meander patterns (20 mm × 20 mm) oriented perpendicular to each other. [Inset: Shows the CAD model of the layered motif, in which each layer is depicted in a different color for visual clarity.]

third embodiment, we produced a three-layer sensor (Figure 4c) modeled after a biaxial strain and pressure sensor, which was originally constructed by micromolding channels of the prescribed design in each layer, laminating those individual layers together, and then manually infilling the embedded channels with e-GaIn.[41] By using e-3DP, this complex sensor design is now produced in a single step, resulting in a fully continuous, monolithic, soft sensor. Finally, to demonstrate the truly freeform capabilities of e-3DP, we produced the 3D tapered spiral shown in Figure S6. Collectively, these demonstrations show how e-3DP offers the ability to pattern conductive inks within soft, highly extensible matrices with nearly arbitrary form factors.

In summary, we report a new method for creating highly stretchable sensors based on embedded 3D printing of a carbon-based resistive ink within an elastomeric matrix. By tuning the rheological properties of the ink, reservoir, and filler fluid, mechanically robust, scalable, and complex sensor designs were fabricated. e-3DP allows for the sensor geometry and properties to be independently tuned by controlling print path and filament cross-section, respectively. Our approach opens new avenues for creating soft functional devices for wearable electronics, human/machine interfaces, soft robotics, and beyond.

Experimental Methods

Materials System: The conductive ink is prepared by homogenizing the as-received carbon conductive grease (MG Chemicals) for two minutes at 2000 rpm in an ARE-310 planetary mixer (Thinky Mixer USA). After mixing, the ink is defoamed in the mixer for an additional two minutes at 2200 rpm. The final ink is loaded into a 3 cc syringe for e-3DP. The elastomeric reservoir is synthesized by mixing 1 Part A Ecoflex 00–30: 1 Part (Part B Ecoflex 00–30 + 2 wt% Slo-Jo Platinum Silicone Cure Retarder) with 1 wt% Thivex. The

filler fluid is produced by mixing 1 Part A: 1 Part (B + 2 wt% Slo-Jo Platinum Silicone Cure Retarder) with 10 wt% Silicone Thinner. (All reagents were purchased from Smooth-On). Thivex and Silicone Thinner are added as rheological modifiers, while Slo-Jo is used to prolong their pot-life to maximize printing time. Once the proper ratios of the constituents are combined, the reservoir and filler fluid are each mixed at 2000 rpm in the ARE-310 for 90 s. Defoaming is performed at 2200 rpm for the same time period. After mixing, the reservoir is poured into a Petri dish coated with mold release agent (Candle Mold Release, ArtMind). The filler fluid is gently layered on top of the reservoir. For thicker parts, such as the three-layer sensor and the tapered helix, enough filler fluid must be added such that there is enough material to penetrate several millimeters into the bulk. For these structures, 1–2 mm of filler fluid is sufficient. A filler fluid layer <0.5 mm in thickness is used for thinner parts such as the strain gauge arrays. After pouring, the entire Petri dish is placed on a vortex mixer until the reservoir/filler fluid are leveled. The same procedure is used to create the glove, except the reservoir is poured into a mold that is preformed into the shape of a hand instead of a Petri dish.

Rheology Characterization: The rheological properties of the conductive ink, reservoir, and filler fluid are characterized under ambient conditions using a controlled stress rheometer (Discovery HR-3 Hybrid Rheometer, TA Instruments). A 40 mm tapered cone plate geometry (2.005°, 56 μm truncation gap) and a 40 mm disposable parallel plate geometry with 200 μm gap are used when studying the conductive ink and uncured, modified Ecoflex-based materials, respectively. Prior to rheological characterization, the conductive ink is mixed in the ARE-310 for 5 minutes at 2000 rpm. Rheological measurements are obtained on the reservoir and filler fluids within 20 minutes of their preparation. Viscometry measurements are carried out over shear rates from 0.01 to 4000 s^{-1}, while oscillatory measurements are carried out at a frequency of 1 Hz within the stress range of 0.1 to 2000 Pa.

Modulus decay testing was performed by cycling the ink at 1 Hz with a strain amplitude corresponding to the strain levels reported in Figure 2c. Modulus recovery testing was performed by cycling the ink at 1 Hz at 100% strain for the number of cycles indicated in Figure S4. After cycling for the specified number of cycles, the applied strain was reduced to 0.01% strain and G' was monitored as a function of time for 15 hours. All moduli values were normalized by G' in the unyielded condition – 119220 Pa (from Figure 2c at 0.1% strain). A 40 mm tapered cone plate geometry (2.005°, 56 μm truncation gap) was used for both the moduli decay and rebuilding tests.

Embedded 3D Printing: All printed sensors and devices are produced using a custom-built 3D printer (ABG 10000, Aerotech Inc.) that translates the conductive ink-loaded syringe through the reservoir. All print paths except for the out-of-plane spiral are generated by writing the appropriate G-code commands. The print path for the out-of-plane spiral shown in Figure S5 is created using CAD software (AutoCAD 2013, Autodesk), which is then translated into G-code using CADFusion (Aerotech). The ink is extruded through a 410 μm inner diameter nozzle (Nordson EFD) by applying the appropriate pressure, which is controlled using an Ultimus V control apparatus (Nordson EFD).

Sensor Performance: The sensors are mounted on a mechanical tester (Instron 5544A, Instron) and stretched at various crosshead speeds (2.96 mm/s for cyclic testing, 23 mm/s for step testing, and 5 mm/s for ultimate strain testing). For the cyclic test, all sensors are elongated to 100% strain. Step tests were performed at 100%, 50%, 5%, and 0.5% strain. Ultimate strain specimens are extended to failure. A good electrical connection is achieved by piercing the sensors' contact pads with a pin soldered to wires. The wires are then connected to a voltage divider, and a voltage corresponding to the resistance change of the sensor is acquired by the voltage input of the load frame.

Their gauge factor is determined by fitting a linear regression to the normalized resistance change as a function of mechanical strain data for each soft sensor for one loading cycle up to 100% strain (crosshead speed of 2.96 mm/s). The slope of the regression corresponded to the gauge factor of the sensor. The reported value represents the average and standard deviation acquired from 15 different sensors (three sensors of each type).

Supporting Information

Supporting Information is available from the Wiley Online Library or from the author.

Acknowledgments

The authors gratefully acknowledge support provided from the National Science Foundation (Grant# DMR-1305284 and Grant# IIS-1226075) and the Wyss Institute for Biologically Inspired Engineering. J. T. M. and R. L. T. are supported by National Science Foundation Graduate Research Fellowships.

Received: January 22, 2014
Revised: May 9, 2014
Published online: June 16, 2014

[1] T. Yamada, Y. Hayamizu, Y. Yamamoto, Y. Yomogida, A. Izadi-Najafabadi, D. N. Futaba, K. Hata, *Nat. Nanotechnol.* **2011**, *6*, 296.
[2] D. Kim, N. Lu, R. Ma, Y. Kim, R. Kim, S. Wang, J. Wu, S. M. Won, H. Tao, A. Islam, K. J. Yu, T. Kim, R. Chowdhury, M. Ying, L. Xu, M. Li, H. Chung, H. Keum, M. McCormick, P. Liu, Y. Zhang, F. G. Omenetto, Y. Huang, T. Coleman, J. A. Rogers, *Science* **2011**, *333*, 838.
[3] C. Pang, G. Lee, T. Kim, S. M. Kim, H. N. Kim, S. Ahn, K. Suh, *Nat. Mater.* **2012**, *11*, 795.
[4] N. Lu, C. Lu, S. Yang, J. A. Rogers, *Adv. Funct. Mater.* **2012**, *22*, 4044.
[5] D. Kim, Y. Kim, J. Wu, Z. Liu, J. Song, H. Kim, Y. Y. Huang, K. Hwang, J. A. Rogers, *Adv. Mater.* **2009**, *21*, 3703.
[6] S. Xu, Y. Zhang, L. Jia, K. E. Mathewson, K. Jang, J. Kim, H. Fu, X. Huang, P. Chava, R. Wang, S. Bhole, L. Wang, Y. J. Na, Y. Guan, M. Flavin, Z. Han, Y. Huang, J. A. Rogers, *Science*. **2014**, *344*, 70.
[7] H. C. Ko, M. P. Stoykovich, J. Song, V. Malyarchuk, W. M. Choi, C. Yu, J. B. Geddes III, J. Xiao, S. Wang, Y. Huang, J. A. Rogers, *Nature* **2008**, *454*, 748.
[8] D. Kim, R. Ghaffari, N. Lu, J. A. Rogers, *Annu. Rev. Biomed. Eng.* **2012**, *14*, 113.
[9] A. Levi, M. Piovanelli, S. Furlan, B. Mazzolai, L. Beccai, *Sensors* **2013**, *13*, 6578.
[10] R. V. Martinez, J. L. Branch, C. R. Fish, L. Jin, R. F. Shepherd, R. M. D. Nunes, Z. Suo, G. M. Whitesides, *Adv. Mater.* **2013**, *25*, 205.
[11] R. F. Shepherd, F. Ilievski, W. Choi, S. A. Morin, A. A. Stokes, A. D. Mazzeo, X. Chen, M. Wang, G. M. Whitesides, *Proc. Natl. Acad. Sci. USA* **2011**, *108*, 20400.
[12] J. C. Nawroth, H. Lee, A. W. Feinberg, C. M. Ripplinger, M. L. McCain, A. Grosberg, J. O. Dabiri, K. K. Parker, *Nat. Biotechnol.* **2012**, *30*, 792.
[13] T. Sekitani, T. Someya, *Adv. Mater.* **2010**, *22*, 2228.
[14] T. Sekitani, H. Nakajima, H. Maeda, T. Fukushima, T. Aida, K. Hata, T. Someya, *Nat. Mater.* **2009**, *8*, 494.
[15] C. Keplinger, J. Sun, C. C. Foo, P. Rothemund, G. M. Whitesides, Z. Suo, *Science* **2013**, *341*, 984.
[16] J. So, J. Thelen, A. Qusba, G. J. Hayes, G. Lazzi, M. D. Dickey, *Adv. Funct. Mater.* **2009**, *19*, 3632.
[17] C. Ladd, J. So, J. Muth, M. D. Dickey, *Adv. Mater.* **2013**, *25*, 5081.
[18] B. C.-K. Tee, C. Wang, R. Allen, Z. Bao, *Nat. Nanotechnol.* **2012**, *7*, 825.
[19] S. Rosset, H. R. Shea, *Appl. Phys. A-Mater.* **2013**, *110*, 281.
[20] S. Rosset, M. Niklaus, P. Dubois, H. R. Shea, *Adv. Funct. Mater.* **2009**, *19*, 470.

[21] D. P. J. Cotton, I. M. Graz, S. P. Lacour, *IEEE Sens. J.* **2009**, *9*, 2008.
[22] M. L. Hammock, A. Chortos, B. C. K. Tee, J. B. H. Tok, Z. Bao, *Adv. Mater.* **2013**, *25*, 5997.
[23] C. Pang, C. Lee, K. Suh, *J. Appl. Polym. Sci.* **2013**, *130*, 1429.
[24] J. A. Rogers, T. Someya, Y. Huang, *Science* **2010**, *327*, 1603.
[25] C. Mattmann, F. Clemens, G. Tröster, *Sensors* **2008**, *8*, 3719.
[26] C. Cochrane, V. Koncar, M. Lewandowski, C. Dufour, *Sensors* **2007**, *7*, 473.
[27] C. Lee, L. Jug, E. Meng, *Appl. Phys. Lett.* **2013**, *102*, 183511.
[28] C. Yan, J. Wang, W. Kang, M. Cui, X. Wang, C. Y. Foo, K. J. Chee, P. S. Lee, *Adv. Mater.* **2014**, *26*, 2022.
[29] X. Niu, S. Peng, L. Liu, W. Wen, P. Sheng, *Adv. Mater.* **2007**, *19*, 2682.
[30] D. Kim, J. Xiao, J. Song, Y. Huang, J. A. Rogers, *Adv. Mater.* **2010**, *22*, 2108.
[31] D. Kim, J. Song, W. M. Choi, H. Kim, R. Kim, Z. Liu, Y. Y. Huang, K. Hwang, Y. Zhang, J. A. Rogers, *Proc. Natl. Acad. Sci. USA* **2008**, *105*, 18675.
[32] I. M. Graz, S. P. Lacour, *Appl. Phys. Lett.* **2009**, *95*, 243305.
[33] K. Chun, Y. Oh, J. Rho, J. Ahn, Y. Kim, H. R. Choi, S. Baik, *Nat. Nanotechnol.* **2010**, *5*, 853.
[34] T. Sekitani, Y. Noguchi, K. Hata, T. Fukushima, T. Aida, T. Someya, *Science* **2008**, *321*, 1468.
[35] A. P. Robinson, I. Minev, I. M. Graz, S. P. Lacour, *Langmuir* **2011**, *27*, 4279.
[36] F. Xu, Y. Zhu, *Adv. Mater.* **2012**, *24*, 5117.
[37] W. Hu, X. Niu, R. Zhao, Q. Pei, *Appl. Phys. Lett.* **2013**, *102*, 083303.
[38] M. Park, J. Im, M. Shin, Y. Min, J. Park, H. Cho, S. Park, M. Shim, S. Jeon, D. Chung, J. Bae, J. Park, U. Jeong, K. Kim, *Nat. Nanotechnol.* **2012**, *7*, 803.
[39] D. J. Lipomi, M. Vosgueritchian, B. C. K. Tee, S. L. Hellstrom, J. A. Lee, C. H. Fox, Z. Bao, *Nat. Nanotechnol.* **2011**, *6*, 788.
[40] D. M. Vogt, Y. Park, R. J. Wood, *IEEE Sens. J.* **2013**, *13*, 4056.
[41] Y. Park, B. Chen, R. J. Wood, *IEEE Sens. J.* **2012**, *12*, 2711.
[42] Y. Park, C. Majidi, R. Kramer, P. Bérard, R. J. Wood, *J. Micromech. Microeng.* **2010**, *20*, 125029.
[43] C. Majidi, R. Kramer, R. J. Wood, *Smart Mater. Struct.* **2011**, *20*, 105017.
[44] J. Chossat, Y. Park, R. J. Wood, V. Duchaine, *IEEE Sens. J.* **2013**, *13*, 3405.
[45] W. Wu, A. DeConinck, J. A. Lewis, *Adv. Mater.* **2011**, *23*, H178.
[46] According to the manufacturer's data sheet: Ecoflex, http://www.smooth-on.com/index.php?cPath = 1130 (accessed June 2013).
[47] According to the manufacturer's data sheet: Carbon Conductive Grease, http://www.mgchemicals.com/products/greases-and-lubricants/conductive-greases/carbon-conductive-grease-846/ (accessed June 2013).
[48] According to the manufacturer's data sheet: CircuitWorks Carbon Conductive Grease 7200, http://www.all-spec.com/downloads/circuitworks/CW7200_060612s.pdf (accessed April 2014).
[49] According to the manufacturer's data sheet: Nyogel 758G, http://www.nyelubricants.com/products/elec_conductive.shtml (accessed April 2014).
[50] W. B. Dobie, P. C. Isaac, *Electric Resistance Strain Gauges* English Universities Press Limited, **1947**.
[51] N. Stübler, J. Fritzche, M. Klüppel, *Polym. Eng. Sci.* **2011**, *51*, 1206.
[52] P. Wang, T. Ding, *J. Mater Sci.* **2010**, *45*, 3595.
[53] S. Wang, P. Wang, T. Ding, *Polym. Composite.* **2011**, *32*, 29.
[54] J. S. Bergström, M. C. Boyce, *J. Mech. Phys. Solids* **1998**, *46*, 931.
[55] Y. L. Park, D. Tepayotl-Ramirez, R. J. Wood, C. Majidi, *Appl. Phys. Lett.* **2012**, *101*, 191904.
[56] S. Michel, X. Q. Zhang, M. Wissler, C. Lowe, G. Kovacs, *Polym. Int.* **2010**, *59*, 391.